Phase behaviour and dynamical features of a two-dimensional binary mixture of active/passive spherical particles

Diego Rogel Rodriguez, 1,2 Francisco Alarcon, 1,2 Raul Martinez, 1,2,3 Jorge Ramírez, 4 and Chantal Valeriani 1,2 ¹⁾Departamento de Estructura de la Materia, Fisica Termica y Electronica, Universidad Complutense de Madrid, 28040 Madrid, Spain
²⁾GISC - Grupo Interdisciplinar de Sistemas Complejos 28040 Madrid, Spain.

In this work we have characterized the phase behaviour and the dynamics of bidimensional mixtures of active and passive Brownian particles. We have evaluated state diagrams at several concentrations of the passive components finding that, while passive agents tend to hinder phase separation, active agents force crystal-like structures on passive colloids. In order to study how passive particles affect the dynamics of the mixture, we have computed the long-time diffusion coefficient of each species, concluding that active particles induce activity and super-diffusive behaviour on passive ones. Interestingly, at the density at which the system enters a MIPS state the active particles' diffusivity shows an inflection point and the passive particles' one goes through a maximum, due to the change in the dynamics of the active components, as shown in the displacement's probability distribution function.

Introduction

Active matter systems are composed of constituents that consume energy in order to move or exert mechanical forces, constantly driving themselves away from equilibrium². Examples of active particles at the mesoscopic scale are living, such as bacteria, or artificial, such as active colloids^{3,4}. In these systems, the violation of time reversal symmetry, which is the main feature of non-equilibrium dynamics, occurs at the level of individual components, unlike driven systems such as granular matter or thermophoretic colloids, in which the departure from equilibrium is due to external fields or boundary conditions. One of the characteristic features of active matter is collective motion, i.e. a behaviour in which the action of an individual unit is dominated by the influence of other components. The collective behavior can be originated from the deviation from equilibrium, leading to novel phenomena such as nonequilibrium phase transitions or large scale directed motion⁵.

Experiments on spherical man-made self-propelling colloids have shown that active particles can present interesting emergent collective properties⁶⁻⁸, such as motility-induced phase separation (MIPS). This phase separation involves the spontaneous assembly of particles due to the persistence of their direction of motion, forming a stable dense and dilute phase even in the absence of an explicit attraction or aligning interactions⁹. An example of active particles undergoing MIPS under suitable conditions are Active Brownian Particles (ABP), i.e. self-propelled Brownian particles that could interact with each other via a purely repulsive potential. To understand the basic microscopical mechanism underlying MIPS in ABP, it is important to study the time it takes a particle to reorient its direction of motion with respect to the thermal noise^{10,11,22}

Systems formed by a mixture of active and passive Brownian colloids provide a novel way for switchable selfassembly¹³, micro-rheological measurements¹⁴, or help understanding active dynamical processes within the cell¹⁵. For this reason, their structural properties and phase behaviour have been recently the subject of a few studies, mostly focused on the formation of MIPS^{16,17}.

The goal of our work is to characterise both the phase behaviour and the dynamics of a two dimensional binary mixture of active and passive Brownian particles. For the former, we will numerically study a mixture of monodisperse active/passive spheres, to establish phase separation within a broad parameter space (density, Péclet and fraction of passive particles). For the latter, we will compute the diffusion coefficient of both passive and active colloids together with the displacement's probability distribution function. Our findings can be considered relevant to the design of experimental devices that pursue the driven self-assembly of passive colloids, such as the ones used in microrheological measurements¹⁴, or shed light upon the behaviour of active matter in heterogeneous media.

The manuscript is organised as follows. In section II we present the simulation details and the tools used to characterise both structure and dynamics. In section III we present our results for the structural properties and in section IV for the dynamical features. Finally, we discuss our conclusions in section V.

NUMERICAL METHODS

In order to study the binary mixture of active/passive particles, we perform Brownian Dynamics simulations with an in house modified version of the LAMMPS²⁰ open source package. The system consists of $N = N_a + N_p$ spherical colloids in a two-dimensional box of size L with periodic boundary conditions, where N_a is the number of active colloids and N_p is the number of passive colloids. It is a monodisperse mixtures, with diameter σ .

All particles undergo a translational Brownian motion (eq.1), where active particles are characterised by an addi-

³⁾Departamento de Física Teórica de la Materia Condensada, Facultad de Ciencias, Universidad Autónoma de Madrid, 28049 Madrid, Spain.

⁴⁾Departamento de Ingeniería Química, ETSI Industriales, Universidad Politécnica de Madrid, 28006 Madrid,

tional constant self-propelling force F_a acting along the orientation vector \vec{n}_i . Besides translation, the orientation vector of active particles evolves according to a rotational diffusion equation (eq. 2).

$$\dot{\vec{r}}_i = \frac{D}{k_B T} \left(-\sum_{j \neq i} \nabla V(r_{ij}) + |F_a| \vec{n}_i \right) + \sqrt{2D} \, \vec{\xi}_i, \tag{1}$$

$$\dot{\theta}_i = \sqrt{2D_r} \, \xi_{i,\theta},\tag{2}$$

where $V(r_{ij})$ is the interparticle pair potential, k_B is the Boltzmann constant, T is the temperature, and the components of $\vec{\xi}_i$ and $\xi_{i,\theta}$ are white noise with zero mean and correlations $\langle \xi_i^{\alpha}(t) \xi_j^{\beta}(t') \rangle = \delta_{ij} \delta_{\alpha\beta} \delta(t-t')$. The translational, D, and rotational, D_r , diffusion coefficients obey the Stokes-Einstein relation¹⁸: $D_r = 3D/\sigma^2$. Both passive and active particles interact with each other via a purely repulsive WCA potential¹⁹.

$$V(r) = \begin{cases} 4\varepsilon \left(\left(\frac{\sigma}{r} \right)^{12} - \left(\frac{\sigma}{r} \right)^{6} \right) + \varepsilon, & r < 2^{1/6}\sigma \\ 0, & r \ge 2^{1/6}\sigma \end{cases}$$
(3)

where ε has energy dimensions, r is the center to center distance, and σ the particles' diameter. Throughout this study, we have used reduced units, in which lengths, times and energies are given in terms of $\sigma = 1$, $\tau = \sigma^2/D$, $k_BT = 1$ and D = 1, and set $\varepsilon = k_BT$. The time step has been set to $\Delta t = 10^{-5}\tau$.

As a measure of the degree of activity, we use the Péclet number, an adimensional number defined as

$$Pe = \frac{3v}{\sigma D_r},\tag{4}$$

where $v = |F_a|D/k_BT$ is the self-propelling velocity. If Pe \ll 1, the particle's motion is governed by diffusion, as for passive Brownian particles, while for Pe \gg 1 diffusive transport is negligible compared to active motion.

In this study we systematically change the Pe number, the density of particles ($\rho = N/(L^2)$) and the ratio between active and passive particles. We choose to work with the total number density ρ (instead of the area fraction ϕ), as it is a magnitude that does not depend on the particle's diameter, as we will comment later in the text.

When focusing on motility induced phase separation in a monodisperse mixture we consider system's sizes ranging from N = 90000 to N = 180000, setting the box lenght L accordingly to obtain the desired total number density.

In order to detect phase separation, we have implemented a standard Voronoi cell method to measure local number density²¹. This method involves computing a Voronoi tessellation over the simulation box, where each colloid is in a corresponding Voronoi cell and the local number density ρ is given as the inverse of the area of each cell. We define $P(\rho)$ as the probability distribution of finding a cell with local number density ρ . Typically, an isotropic system (Fig. 1a) shows a $P(\rho)$ with only one local maximum around the total number density ρ (Fig. 1b), whereas a phase separated system (Fig. 1c) shows two local maxima: one centred at the dilute

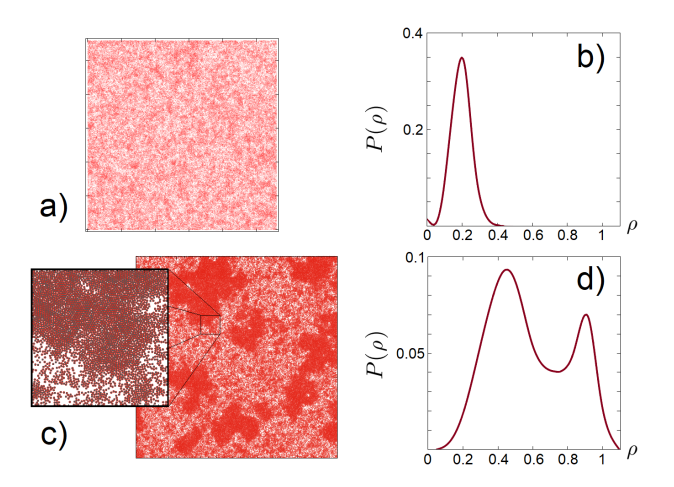


FIG. 1. Snapshots of ABP at $\rho = 0.5$ and $N_p = 0$ showing a) no phase separation (Pe=40), b) its $P(\rho)$ distribution $P(\rho)$ is centered at 0.2 and c) MIPS (Pe=120) and d) its $P(\rho)$ distribution.

phase and another at the concentrated phase (Fig. 1d). Thus, an inspection of $P(\rho)$ will reveal the existence of a motility induced phase separation.

In order to characterize the dynamics of the system, we have computed the long time diffusion coefficient via the mean-square displacement (MSD) of either active or passive particles in the presence of active ones, given by

$$MSD_{a/p}(t) = \frac{1}{N_{a/p}} \sum_{i=1}^{N_{a/p}} (\vec{r}_{a/p,i}(t) - \vec{r}_{a/p,i}(0))^{2}.$$
 (5)

Moreover, we have also computed the probability distribution function of particles' displacements for either passive and active particles.

II. RESULTS

To unravel the role played by passive colloids in a suspension of active agents we estimate in Fig. 2 ρ -Pe state diagrams for a wide range of Péclet numbers, total number densities ρ , and fraction of passive particles N_p/N . The reason behind using the total number density instead of the packing fraction has been already suggested in Ref.^{27,31}: when changing the propulsion force implies changing the Peclet number, when increasing Pe particles end up colliding at a very high speed, thus decreasing their effective diameter.

As shown in Fig.2, we mostly focused on relatively large Peclet numbers (larger than 40). Interestingly, for lower values of Pe the authors of Ref.¹ demonstrated the existence of a coexistence between an active liquid and a hexatic phase in a two dimensional suspension of Active Brownian Particles.

For purely active systems (dashed black line) and systems with the lowest fractions of passive particles (in red), MIPS are formed when densities are at least $\rho \sim 0.5$ (corresponding to $\phi \sim 0.4$) and Pe ranging from 60 (at the highest densities) to 80 (at the lowest densities). When comparing to the

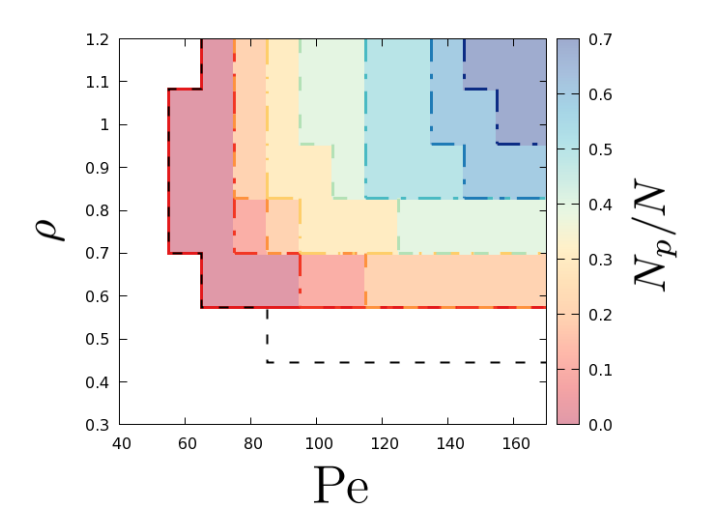


FIG. 2. ρ -Pe state diagrams of monodisperse mixtures of active/passive particles. Coloured areas correspond to MIPS, different colours representing different fractions N_p/N of passive components. Black dashed line is for purely active WCA particles from Ref.²⁷.

state diagram presented by Stenhammar *et al.*²⁷ (black dashed line in the figure), we detect a small difference when $\rho \sim 0.5$ ($\phi \sim 0.4$) This is due to the different definition of Peclet number adopted in our work and in their work: while in our work D_r is set to 3 and the self-propelling velocity is changed in order to vary the Péclet number, Stenhammar *et al.*. vary Pe by fixing v and varying k_BT and so D_r . As we will present below, at high Péclet numbers, our definition effectively reduces the particle diameter and, therefore, the area fraction of particles in the system. However, when following the same procedure as Stenhammar, we recovered their results, with MIPS at number densities of $\rho \sim 0.5$ and Péclet =90 and above (see Appendix).

Adding passive components shifts the state diagram to higher values of Pe and ρ simultaneously: higher densities and activities are needed to get phase separated systems. Even though passive components tend to hinder phase separation, MIPS are detected even in systems containing up to 70% of passive particles, whenever the self-propelling velocity of active components and the total density are high enough. On the contrary, MIPS have not been observed at higher fractions of passive agents in the range of Péclet numbers considered in this work (up to Pe = 250).

The authors of Ref.¹⁶ studied mixtures of active and passive particles and derived a relationship between density and Pe number ($\phi_0 \sim 1/Pe$) using the kinetic model developed in³²: they concluded that this relationship was capable of fitting the results for ABP simulations when $\phi > 0.4$ and $N_p/N = 0.5$. We observe that all MIPS regions can be scaled one on top of another.

Differently from Ref. ¹⁶, the MIPS boundaries in Fig. 2 have a similar parabolic-like shape culminating in what could be identified as a critical point (Pe₀, ρ_0) for every value of N_p/N . With this idea in mind, we approximately estimate the location of Pe₀ and ρ_0 for every fraction N_p/N of passive particles.

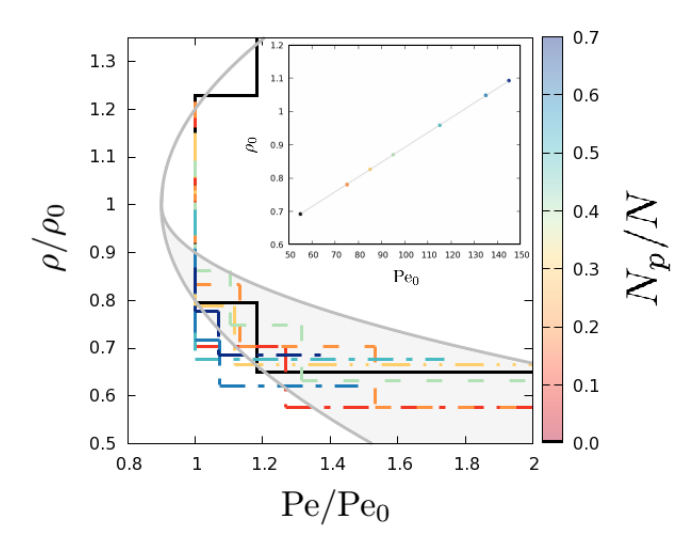


FIG. 3. State diagrams (coloured lines) as in Fig. 2 where ρ and Pe have been normalized by the estimated values of ρ_0 and Pe₀ for each N_p/N . Black line (purely active case). Gray curves: dispersion estimated fitting the state diagrams to a binodal curve. Inset: linear behaviour of ρ_0 versus Pe₀.

Fig. 3 shows the normalized phase diagrams of monodisperse mixtures when the curve for the purely active case (black line, $N_p/N=0$) is taken as reference. All curves seem to collapse onto a master curve when representing them as a function of ρ/ρ_0 vs Pe/Pe₀.

Interestingly, the critical points ρ_0 , Pe₀ for the different passive fractions are aligned, as shown in the inset of Fig. 2. On the one side, this might allow us to predict, for every concentration of passive particles up to close packing, the maximum Peclet beyond which MIPS can be detected (being $\rho = 1.15$ the maximum close packing density). On the other side, this suggests that the normalised state diagrams for active/passive binary mixtures are very similar at every N_n/N , for mixtures with up to 70% of passive particles. Beyond that ratio, the overall density needed to observe MIPS is so high that the mixture behaves as a very dense suspension of passive particles, where particles interact repulsively and MIPS are absent. Therefore, given that the rescaled state diagrams for low/moderate fractions of passive particles are similar, one might wonder whether the structure of MIPS (whenever it occurs) may also be similar.

In the top panels of Fig. 4, we compare the snapshots of two different MIPS cases, corresponding to a) high passive particle concentration $(N_p/N=0.6, \text{Pe}=190, \rho=1.018, \text{deep})$ into the blue region of Fig. 2) and b) low passive particle concentration $(N_p/N=0.3, \text{Pe}=170, \rho=0.891, \text{deep})$ into the yellow region of Fig. 2). In either case, the denser phase is formed by a skin of active colloids (in red) encapsulating the passive ones (in blue), even when the passive particles' concentration is lower (panel b). When analysing the phase-separated mixture in more detail, we observe that the self-assembly of the dense phase is triggered by active fronts that trap the passive components, favouring the spontaneous aggregation of passive agents. However, in the dilute phase the

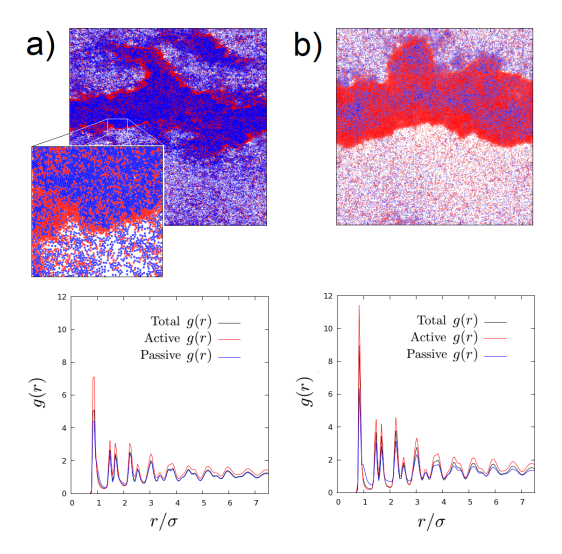


FIG. 4. Top: snapshots of monodisperse phase-separated mixtures of passive (blue)/active (red) colloids: a) $N_p/N = 0.6$, $\rho = 1.018$, Pe = 190, b) $N_p/N = 0.3$, $\rho = 0.891$, Pe = 170. Bottom: radial distribution functions corresponding to the top panels.

distribution of passive and active particles is more homogenous

As shown by the partial pair distribution function g(r) for active and passive colloids (Fig. 4-bottom panels), crystallike structures are present at short distances, and liquid-like at longer distances. However, the partial g(r) for active particles reveals a structure that is better defined than the one for passive agents. Given that passive particles would never show the same structuring in the absence of active agents, one could conclude that active particles force clustering of passive ones, as if an effective attraction was present between them. The partial radial distribution functions for active/passive colloids show a first high peak, indicating that both types of colloids are strongly packed, at $r < \sigma$. The reason is that in order to alter the Pe we change the self-propelling speed of the active particles. This reduces the effective particle radius when activity increases, being the WCA a not-too stiff interaction potential. This result motivated our choice of adopting ρ as the measure of density, instead of the area fraction used in Ref.²⁷.

In order to better unravel possible differences between MIPS at different concentration of passive particles, we focus on one point of the state diagram (Pe = 120, ρ = 1.018 in Fig. 2) where most of the different N_p/N fractions show MIPS. Fig. 5 shows a set of snapshots for several fractions of passive particles, ranging from the lowest N_p/N (panel a) to the highest N_p/N (panel g). While in most cases the state point is well in the MIPS region ($N_p/N = 0.1$ (panel a), $N_p/N = 0.2$ (panel b), $N_p/N = 0.3$ (panel c), $N_p/N = 0.4$ (panel d), $N_p/N = 0.5$ (panel e), $N_p/N = 0.6$ (panel f)), the case corresponding to $N_p/N = 0.7$ (panel g) lies outside its corresponding MIPS boundaries. We note that, when increasing the amount of passive particles, the system tends to form many smaller clusters until a maximum threshold for N_p/N is reached, for which the active agents can no longer trap passive particles and are

unable to trigger MIPS. Furthermore, density fluctuations in these mixtures are larger than in the purely active systems. While purely active systems maintain a relatively stable phase separation (as shown in panel a, very close to a purely active case), clusters in mixtures of active and passive colloids are more dynamic, since they are permanently moving, vanishing and remerging (see videos in the supplementary information).

When studying the local number density distribution functions $P(\rho)$ of active/passive particles associated with MIPS, we notice an interesting behaviour in the way the $P(\rho)$ evolves as a function of ρ and Pe. While a system consisting of only passive particles (without active agents) presents a gaussian $P(\rho)$ distribution centred around the total number density, the shape of the $P(\rho)$ can be strongly affected by the amount of active particles added to the suspension. Fig. 6(a) shows a series of $P(\rho)$ (right panel) of systems at different nominal densities, each one next to the MIPS boundaries, depending on N_p/N and at a fixed Pe of 120 (left panel). For purely active (red) and systems with N_p/N up to about 0.5 (light green) a clear phase separation appears, with two well defined peaks at low and high densities, respectively. This corresponds to the encapsulating mechanism in MIPS (observed in Fig.4 and 5), in which passive particles are trapped in a dense phase by the active colloids, while the rest of them remain in a low density phase. Increasing N_p/N even further leads to a less pronounced phase separation, with the two peaks merging each other around the nominal total density (as shown in panels e and f of Fig. 5).

Fig. 6(b) shows a series of $P(\rho)$ (right panel) for phase separated systems, fixing $\rho=1.018$ and varying Pe (left panel). We notice that, as N_p/N increases the distance between the two local maxima in $P(\rho)$ decreases, as well as the height of the dense phase local maxima. In addition, the low-density phase becomes more populated and shifts towards $\rho=1.018$ as N_p/N increases. All of this suggests that the mixture is increasingly more homogeneous when increasing the fraction of passive particles in the system, a phenomenon also noticeable in the snapshots from Fig. 5.

Inspecting Fig. 6 in more detail, it is interesting to note how the lever rule, which is frequently used to determine the fraction of high and low density phases at equilibrium in systems involving two phases, seems to work also in the case of mixtures of active and passive ABP. On the one hand, in Fig. 6(b), the point corresponding to $N_p/N=0.1$ has a density ρ which is larger than the critical density ρ_0 corresponding to that fraction of passive particles, and thus is closer to the high density binodal curve. The accompanying $P(\rho)$ shows that a much higher fraction of particles can be found in a high density phase. On the other hand, the point corresponding to $N_p/N=0.7$ has a ρ which is smaller than the corresponding critical density ρ_0 . In that case, the related $P(\rho)$ shows that most particles can be found in a low density phase.

It has been already shown that in the case of a pure ABP suspension the system is characterised by an effective diffusivity $D_e(\rho)$ that depends on density²⁴. Thus, one should expect also an effective diffusivity for passive particles in a bath of active ones, which could depend not only on the self-propel velocity of the active particles but also on the total density and

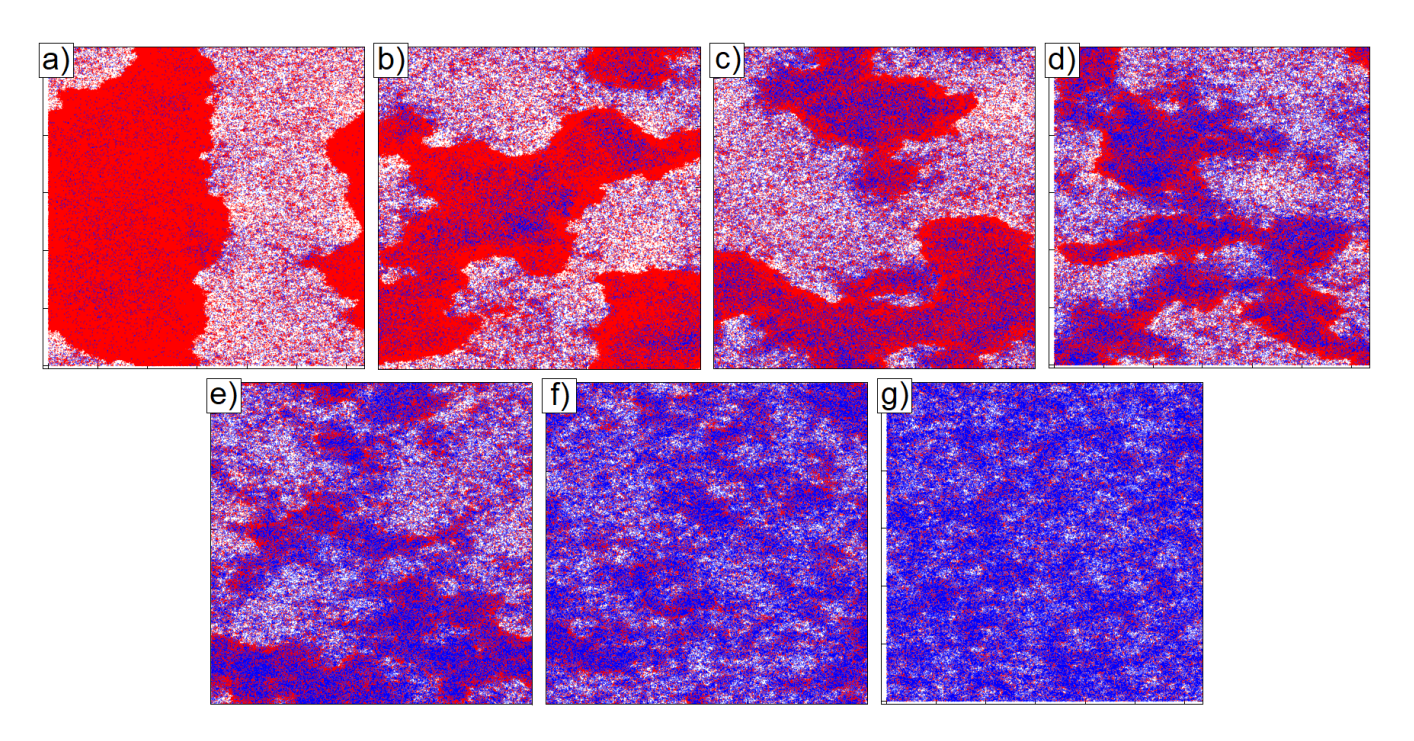


FIG. 5. a-g) Snapshots at $\rho = 1.018$, Pe = 120 and several N_p/N fractions (passive particles in blue and active ones in red): a) $N_p/N = 0.1$ b) $N_p/N = 0.2$ c) $N_p/N = 0.3$ d) $N_p/N = 0.4$ e) $N_p/N = 0.5$ f) $N_p/N = 0.6$ g) $N_p/N = 0.7$. a), b), c), d), e) and f) show MIPS, while in g), the high N_p/N forbids MIPS. Movies of panel b), d) and e) can be found in the Supplementary Information.

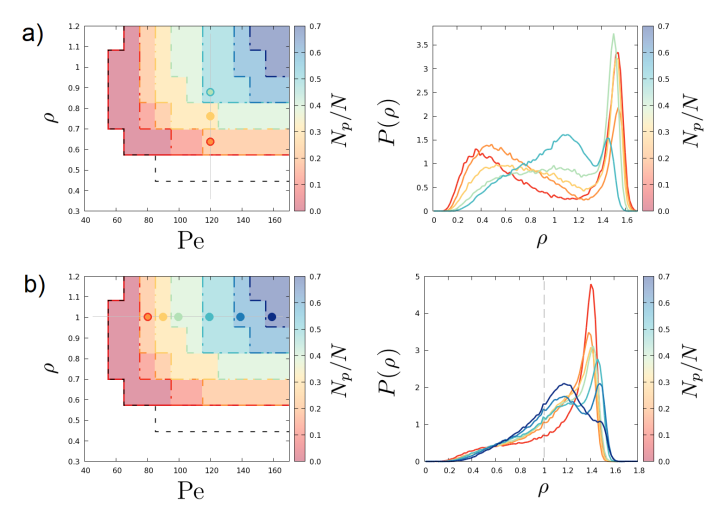


FIG. 6. Right panel: local number density distributions $P(\rho)$ for systems at the MIPS boundaries for a) a constant Péclet number of Pe= 120, b) a constant number density of $\rho=1.018$. Left panel: phase diagrams of monodisperse mixtures of active/passive colloids, with coloured circles indicating the ρ and Pe conditions for which its corresponding $P(\rho)$ is shown.

fraction of passive particles in the system.

In order to unravel how passive particles affect the dynamics of active ones (and viceversa) in the MIPS region, we compute the long-time diffusion coefficient from the MSD of each species at different passive particles concentrations (Fig.7) fixing the value of the Peclet number (Pe = 120). This value

corresponds to the one already chosen in Fig.6 a) to study how the appearance of MIPS is affected by the different N_p/N .

The top panel of Fig.7 represents the active particles' diffusion as a function of density. At the density at which MIPS appears, either in purely active (red) or in systems with N_p/N up to about 0.5 (light green), the diffusion coefficient changes its slope and we detect different scenarios. At low density, where MIPS does not take place, active particles freely diffuse (the lower the density the higher the diffusion). When MIPS starts appearing in the system (as an example, $\rho \sim 0.5$ in the $N_p/N=0.1$ case), many active particles move to the boundaries of the densest phase and their diffusion coefficient decreases (the higher the density the slower particles diffuse). When the presence of MIPS is debatable $(N_p/N=0.7)$ and high densities), active particles diffuse very slowly.

The bottom panel of Fig.7 represents the passive particles' diffusion coefficient at the same conditions as in panel a, having set the same Pe = 120 for active particles. To start with, the passive particles' diffusion is almost two order of magnitude lower than the active particles' one. When the density increases, as soon as the system enters into the MIPS region, the diffusion coefficient shows a non-monotonic behaviour at the same density where the active particles diffusivity shows an inflection point. This effect is barely visible at very low N_p/N , due to the small number of passive particles in the system, but becomes clearer as soon as $N_p/N = 0.3$. A possible explanation for this is the following. At low densities the system is not phase separated yet, and the diffusivity of passive particles increases as the density increases until the latter reaches the value corresponding to the MIPS boundary. When

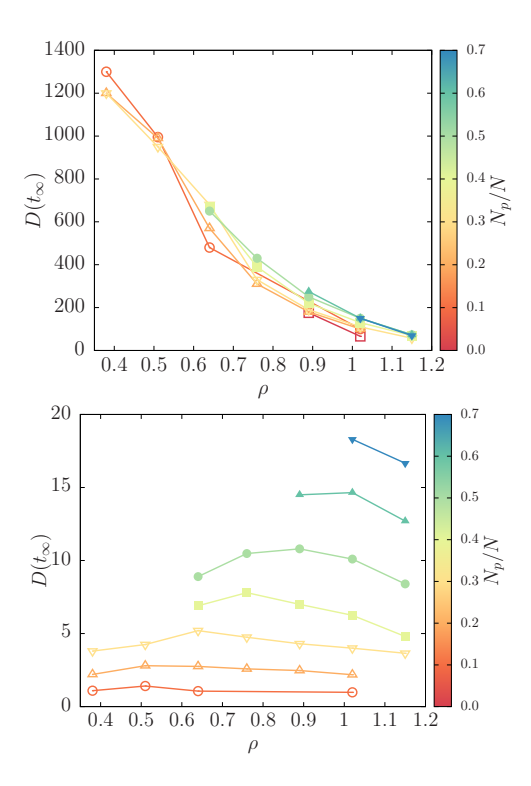


FIG. 7. Long time diffusion coefficient as a function of the total number density for active (top) and passive particles (bottom) at Pe=120 and different passive particles concentration (as shown by the color code), corresponding to the state points shown in Fig,6 a).

the system enters a MIPS region, while active particles start slowing down, passive particles' diffusivity increases as an effective result of the active particles' speed. Once in the MIPS phase, at higher densities, passive particles are trapped by a layer formed by the active ones: this is the reason why their diffusivity decrease. Therefore, we conclude that either an inflection point in the active particles diffusivity (especially at low N_p/N) or a maximum of the passive particles diffusivity (especially at higher N_p/N), when plotted as a function of the total particle density ρ , could be used as a dynamical finger-print for the appearance of MIPS in an active/passive binary mixture.

When active particles are swimmers and passive particles are tracers five times smaller than the swimmers, in the dilute regime *i.e.* ($\rho_{active} < 0.06$ and $\rho_{passive} = 0.0034$), Delmotte et al.³³ have found that the onset of the diffusive regime occurs after a period of anomalous transport at short times, as the active packing fraction of swimmers increases. Even though we are in a more concentrated regime without hydrodynamics and passive particles have the same size as the active particles, we have also found a period of anomalous transport at short times as the number of passive particles increases (not shown here). When studying the system with hydrodynamics, the effective diffusion coefficient of tracers, calculated in the diffusive regime at long times, increases with the swimmers packing fraction in the same way as in the experiments³³. In contrast, without hydrodynamics and in more concentrated regimes, we have found the effective diffusion coefficient of tracers showing a non-monotonic behaviour due to MIPS, see bottom panel of Fig. 7

To further study the dynamics of the mixture, we compute the distribution of particle displacements for both active and passive particles in the steady state (Fig. 8).

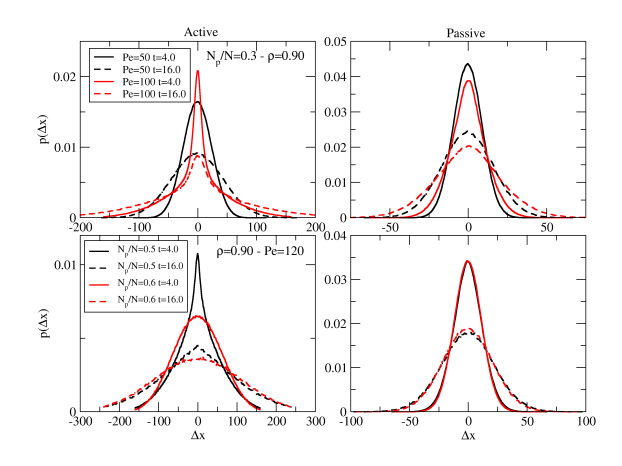


FIG. 8. Probability distribution of the displacements along the x axis measured at different times of active (left) and passive (right panels), in mixtures with $N_p/N=0.3$ and $\rho=0.9$ (top) for Pe=50 (no MIPS) and Pe=100 (MIPS), and in mixtures with $\rho=0.9$ and Pe=120 for $N_p/N=0.5$ (MIPS) and $N_p/N=0.6$ (no MIPS).

In Fig. 8 top panels we focus on the system at $N_p/N=0.3$ and density $\rho=0.90$ outside (Pe=50, in black) and inside (Pe=100, in red) the MIPS state, comparing the $P(\Delta x)$ at short (continuous) and long (dashed) times for both active (left-side) and passive (right-side) particles.

In the passive case, independently on whether the system is in the MIPS state, the $P(\Delta x)$ is always a Gaussian distribution centred in $\Delta x=0$ whose width increases with time. The same happens for active particles when the system is outside a MIPS state. On the contrary, even though the time evolution is the same, the shape of the active particles' $P(\Delta x)$ is clearly non-Gaussian when the system is in a MIPS state. When computing the PDF at intermediate times, active particles in the less dense phase reminds the behaviour of particles following Levy flight dynamics, showing the PDF a well-defined cusp and slowly decaying tails. When averaging with the contribution coming from active particles in the more dense phase, these characteristics are a smeared out but still present.

In order to underline the dependence of our results on the passive particles' concentration, we repeat the same study choosing a state point where the system is in a MIPS state $(N_p/N=0.5,$ in black), compared to the same state point of a system which is right outside the MIPS state $(N_p/N=0.6,$ in red), compute the $P(\Delta x)$ at short (continuous) and long (dashed) times for both active (left-side) and passive (right-side) particles(bottom panels in Fig. 8), and compare to the same state point of a system which is right outside the MIPS state $(N_p/N=0.6,$ in red). Once more, the $P(\Delta x)$ for passive particles is always a Gaussian, whose width increases with time. However, in the active case we detect clear differences,

given that the distribution is clearly not Gaussian when the system is in a MIPS state (in black) and becomes Gaussian increasing the number of passive particles thus exiting a MIPS state.

Therefore, instead of detecting MIPS by computing the local density (via Voronoi tessellation), we suggest a different route based on dynamics. When computing the $P(\Delta x)$ of active particles at intermediate times, when its shape changes from being Gaussian to being non-Gaussian, the system enters a MIPS state. At very long times, active particles move between different clusters, exploring the low density region along the way, and $P(\Delta x)$ returns to a Gaussian.

Delmotte et al. in³³, to study the effect of steric versus hydrodynamic interactions, have carried out simulations of bidisperse suspensions without hydrodynamic interactions and with and without self-propulsion. The complete passive case developed a Gaussian PDF as expected, while the active/passive case without hydrodynamics developed a PDF with non-Gaussian tails. In our case, perhaps the non-Gaussian tails are not observed at this time-scales, but we did see wider tails in our PDFs. This effect might be due to the tracers' size and the simulated densities. Thus, in our case active particles have less entrainment of passive ones, than in the case of Ref.³³ with smaller tracers.

As suggested in supercooled liquids³⁴, a non-Gaussian behaviour of $P(\Delta x)$ corresponds to dynamic heterogeneities in the system, i.e. spatially separated regions of mobile and less mobile particles. When MIPS occurs, most of active particles slow down forming the boundary of the phase separated region, whereas the remaining keeps propelling in the system. Therefore, a change in the shape of $P(\Delta x)$ is linked to a change in particles' dynamics.

III. CONCLUSIONS

In this work we have carried out an extensive study on the role of passive components in presence of ABP for a purely repulsive interacting potential (WCA) in two dimensions. Firstly, we have elaborated state diagrams for several fractions of passive components, unveiling the necessary conditions for MIPS to occur in these binary mixtures. We have found that passive agents tend to hinder phase separation, but MIPS can still be found in binary mixtures, even for contents of passive colloids as high as 70%. All MIPS regions can be scaled on top of another, culminating in what could be identified as a critical point.

Given that the rescaled state diagrams are similar, we studied the structures of MIPS. The underlying mechanism involves the self-assembly of active fronts that encapsulate passive bulks, giving rise to a phase separation for which dense clusters with a skin of active agents surrounding a mainly passive core are found. Thus we observe that active colloids can induce structure of passive components and trigger crystallisation. To better characterise the system's structure, we compute the local number density distribution function, whose shape is strongly affected by the amount of active particles present in the system. We conclude that the mixture is increasingly

more homogeneous when increasing the fraction of passive particles.

In order to study how passive particles affect the dynamics of the mixture, we compute the long-time diffusion coefficient. Interestingly, at the density at which the system enters a MIPS state the active particles' diffusivity shows an inflection point and the passive particles' diffusivity goes through a maximum, due to the change in the dynamics of the active components clearly described by the $P(\Delta x)$.

We believe that our results could help understanding the phenomena occurring in suspensions of particles with heterogeneous activity, shedding light upon the behaviour of active matter in complex media, and can be used to refine microrheological measurements.

CONFLICTS OF INTEREST

There are no conflicts to declare.

ACKNOWLEDGEMENTS

The authors acknowledge funding from Grant FIS2016-78847-P of the MINECO and the UCM/Santander PR26/16-10B-2. Francisco Alarcón acknowledges support from the "Juan de la Cierva" program (FJCI-2017-33580). Raul Martinez acknowledge funding from MINECO (Ministerio de Economía, Industria y Competitividad, Spain) FPI grant BES-2017-081108. The authors acknowledge the computer resources and technical assistance provided by the Centro de Supercomputación y Visualización de Madrid (CeSViMa).

- ¹P Digregorio, D Levis, A Suma, L F. Cugliandolo, G Gonnella, and I Pagonabarraga, *Phys. Rev. Lett.* **121**, 098003 (2018).
- ²C. Bechinger et al. Rev. Mod. Phys. **88**, 045006 (2016).
- ³W.F. Paxton *et al. Chem. Commun.* **441**, 3 (2005).
- ⁴S. Fournier-Bidoz et al. J. Am. Chem. Soc. **126**, 13424 (2004).
- ⁵T. Vicsek, A. Zafeiris *Phys. Rep.* **517**, 3-41, 71-140 (2012).
- ⁶S. Thutupalli, R. Seemann, S. Herminghaus *New J. Phys.* **13**, 073021 (2011).
- ⁷D. Nishiguchi, Masaki S. *Phys. Rev. E* **92**, 052309 (2015).
- ⁸I. Buttinoni, J. Bialké, F. Kümmel, H. Löwen, C. Bechinger, T. Speck. *Phys. Rev. Lett.* **110**, 238301 (2013).
- ⁹M.E. Cates, J. Tailleur. Annu. Rev. of Condens. Matt. Phys. 6, pp. 219-244 (2015).
- ¹⁰MC Marchetti, JF Joanny, S Ramaswamy, TB Liverpool, J Prost, M Rao, ... Reviews of Modern Physics 85, 1143 (2013)
- ¹¹SA Mallory, C Valeriani, A Cacciuto Annual review of physical chemistry 69, 59-79 (2018)
- ¹²F. Sciortino, S. Mossa, E. Zaccarelli, and P. Tartaglia, *Phys. Rev. Lett.* 93, 055701 (2004).
- ¹³L. Angelani et al. Phys. Rev. Lett. **107**, 138302 (2011).
- ¹⁴Y. Peng et al. Phys. Rev. Lett. **116**, 068303 (2016).
- ¹⁵A. Das, A. Polley, M. Rao. *Phys. Rev. Lett.* **116**, 068306.
- ¹⁶J. Stenhammar et al. Phys. Rev. Lett. 114, 018301 (2015).
- ¹⁷S.N. Weber, C.A. Weber, E. Frey. *Phys. Rev. Lett.* **116**, 058301 (2016).
- ¹⁸H. Brenner. J. of Col. Sci.. **20**, 104-122 (1964).
- ¹⁹J.D. Weeks, D. Chandler, H.C. Andersen. *Journ. of Chem. Phys.* 54-12 (1971)
- ²⁰S. Plimpton. *J Comp Phys*, **117**, 1-19 (1995).
- ²¹S. Slotterback, M. Toiya, L. Goff, J. F. Douglas, W. Losert. *Phys. Rev. Lett.* **101**, 258001 (2008).

- ²²C. Bechinger, R. Di Leonardo, H. Löwen, C. Reichhardt, G. Volpe, G. Volpe. Rev. Mod. Phys. 88, 045006 (2016).
- ²³ K. Martens, L. Angelani, R. Di Leonardo, L. Bocquet. Eur. Phys. J. E 35, 1-6 (2012).
- ²⁴Y. Fily and M. C. Marchetti, *Phys. Rev. Lett.* **108**, 235702 (2012),
- ²⁵W. Kob et al. Phys. Rev. Lett. **79**, 2827 (1997).
- ²⁶A. Rahman, *Phys. Rev.* **136**, A405 (1964).
- ²⁷J. Stenhammar et al. Soft Matter, **10**, 1489-1499 (2014).
- ²⁸R. Martínez, F. Alarcón, J. L. Aragonés, C. Valeriani, D. Rogel-Rodríguez. Eur. Phys. J. E, (2018).
- ²⁹I. Theurkauff, C. Cottin-Bizonne, J. Palacci, C. Ybert, L. Bocquet. *Phys. Rev. Lett.* **108**, 268303 (2012).
- ³⁰J. Bialké, H. Lowen, T. Speck. *Journal of Non-Crystalline Solids* 407, 367375 (2015).
- ³¹Y. Fily, S. Henkes, M.C. Marchetti. *Soft Matter* **13**, (2014).
- ³²S. Redner, M.F. Hagan, A. Baskaran. *Phys. Rev. Lett.* **110**, 055701 (2013).
- ³³B. Delmotte, E.E. Keaveny, E. Climent, F. Plouraboué. *IMA Journal of Applied Mathematics* 83, 680-699 (2018).
- ³⁴M S Shell, P G Debenedetti and F H Stillinger. J. Phys.: Condens. Matter 17, S4035 (2005).

IV. APPENDIX

A. Different formation of MIPS for equal Péclet numbers

We have found disagreement between the phase diagram given by Stenhammar *et al.*²⁷ and our phase diagram for purely active systems with WCA interactions. We have observed that the discrepancy is due to our different approach for varying the Péclet number. In this paper D_r is set constant and the self-propelling speed is changed to alter the Péclet number, while Stenhammar *et al.* vary Pe by fixing v and adjusting D_r . We have recovered the results from Stenhammar *et al.* by following their methodology. From an energetic perspective, Pe measures the ratio between the ballistic energy $|F_a|\sigma$ and the thermal energy k_BT . Since we are employing a WCA po-

tential, the effective diameter for the interactions $\sigma_{\rm eff}$ is not the same for all collision energies due to the softness of the potential. If colloids were ideal hard spheres, $\sigma_{\rm eff}$ would be the same for all self-propelling forces of active agents $|F_a|$. This means that, for WCA, changing Pe by varying $|F_a|$ effectively softens the particles as $|F_a|$ grows, reducing their effective diameter and therefore hindering self-assembly and interfering in MIPS, since phase separation would not be found in the limit of point ABP. This presumably explains the differences between both phase diagrams for ABP.

Another aspect to consider in this regard is the role of thermal phenomena in the competition between diffusive behavior and self-propulsion effects, as presented in Section A. Decreasing D_r lessens the mean frecuency in which particle orientation is reset, implying an increase in the amount of time a trapped particle has to wait until it can have a chance to leave the rim of its cluster. In the limit of no rotational diffusion, a blocked active particle will remain pushing towards the cluster, and therefore contributing to its growth. Thus one would expect MIPS to be favored due to the cancellation of diffusive effects when increasing the Péclet number by decreasing D_r .

However, our method suits the one used in previous works, both experimental 8,29 and computational $^{30-32}$, since it is more controllable and reproducible to change the self-propelling velocity (or, equivalently, $|F_a|$) in experiments by changing the chemical properties of the system in which active colloids are interacting than modifying the rotational diffusion. This suggests the need for an extensive study on the characterization of the Péclet number for out of equilibrium systems and for soft potentials, since this number is widely used to describe the competetition between active and diffusive motion 16,17,22,27 but it seems that Pe is not sufficient to describe these systems, since potential steepness comes into play.